A Compact and Broadband 2×2 3-dB Adiabatic Coupler Based on Trapezoidal Subwavelength Gratings

Haoyu Wu, Yaohui Sun, Yue Zhou, Mengjia Lu, Tong Lin, Guohua Hu, Binfeng Yun, and Yiping Cui

***Abstract*—We propose a compact, broadband 2×2 3-dB adiabatic coupler using trapezoidal subwavelength gratings on silicon-on-insulator platform. The proposed device is constructed by two tapered waveguides, which are composed of trapezoidal subwavelength gratings. Broadband 3-dB optical power splitting with a coupling length of 24 μm is achieved by the adiabatic mode evolution of the two lowest order transverse electric modes. By using the finite time difference method, the power splitting ratio better than 3±0.21 dB and the insertion loss less than 0.19 dB are obtained in the wavelength range of 1450 nm to 1650 nm.**

***Index Terms*—Adiabatic coupler, integrated optics, silicon on insulator, subwavelength gratings.**

I. Introduction

OPTICAL couplers are one of the basic components of photonic integrated circuits (PICs), which are widely used in optical switches [1], [2] modulators [3], and mode (de)multiplexers [4], [5]. 2×2 3-dB optical couplers can evenly split input light into two output lights. Directional couplers (DCs) [6], [7], multimode interference (MMI) couplers [8], [9] and adiabatic couplers [10], [11], [12], [13], [14], [15] are three commonly used 3-dB couplers in PIC. Among them, the structures of DCs and MMIs can be compact and the device size is determined by the beat lengths of the two lowest order modes, which are wavelength dependent due to the mode dispersion, and then limits the working bandwidth. As an alternative, adiabatic coupler is working based on the mode evolution, the excited mode is preserved and other modes are not excited during propagation, which means that there is no energy exchanging among different modes. So broader working bandwidth can be achieved. However, the coupling length of adiabatic coupler needs to be long to achieve adiabatic mode evolution, which leads to a large device footprint. In order to shrink the device size and improve the performance, various schemes have been proposed to improve adiabatic optical couplers, such as using shortcuts to adiabaticity [16], fast quasi-adiabatic dynamics [17], inversely tapered mode evolution [18]. However, these schemes are based on conventional strip/ridge waveguides, which still have large mode dispersion on the silicon-on-insulator (SOI) platform, resulting in high performance with long device size or low performance with compact device size.

Conventional subwavelength grating (SWG) is a periodic structure, in which the period of gratings is smaller than π/β, where β is the propagation constant of the optical mode. Typically, SWG can be regarded as a homogeneous material with an equivalent refractive index and light can be propagated as in the conventional optical waveguides. In addition, the equivalent refractive index of the SWG can be changed by altering the duty cycle of the gratings. Conventional SWG has been widely used on the SOI platform to shrink the device size and achieve broad working bandwidth, such as DCs [19], MMIs [20], adiabatic couplers [21], [22], [23], and polarization beam splitters [24], [25]. When SWG is used to construct optical couplers on the SOI platform, the equivalent refractive index of the SWG in the coupling region is smaller than mode effective index of the conventional silicon strip waveguide, resulting in coupling strength enhancing then reducing the coupling length. Furthermore, compared with the conventional silicon strip waveguide, SWG can achieve smaller mode dispersion, which can support broader working bandwidth of the constructed devices.

Compared with conventional SWG, trapezoidal SWG can change the mode field distribution in the optical waveguide and concentrate light on the long parallel side of trapezoidal SWG. In previous work, trapezoidal SWG has been used to achieve curved waveguides [26], [27], spot size converters [28], and mode converters [29]. However, 2×2 3-dB adiabatic optical coupler based on trapezoidal SWG has not yet been demonstrated. In this work, we propose a 2×2 3-dB adiabatic optical coupler based on trapezoidal SWG on the SOI platform. For optical couplers, trapezoidal SWG can regulate the mode field distributions in two coupled waveguides to give larger mode overlap and then enhance the coupling between two waveguides, which results in a more compact device compared with optical couplers based on the conventional SWG. Similarly, the mode dispersion of the optical coupler based on trapezoidal SWG can be smaller as the content of silicon is reduced compared with optical couplers based on conventional silicon stripe/ridge waveguides. By optimizing the structure of the 2×2 3-dB adiabatic optical coupler based on trapezoidal SWG using finite difference time

Manuscript received 25 February 2023; revised 19 April 2023; accepted 8 May 2023. Date of publication 12 May 2023; date of current version 22 May 2023. This work was supported in part by the National Natural Science Foundation of China under Grant 62171118 and in part by the National Natural Science Foundation of China under Grant 62105061. *(Corresponding author: Binfeng Yun.)*

The authors are with the Advanced Photonics Center, Southeast University, Nanjing 210096, China (e-mail: ybf@seu.edu.cn).

Digital Object Identifier 10.1109/JPHOT.2023.3275709

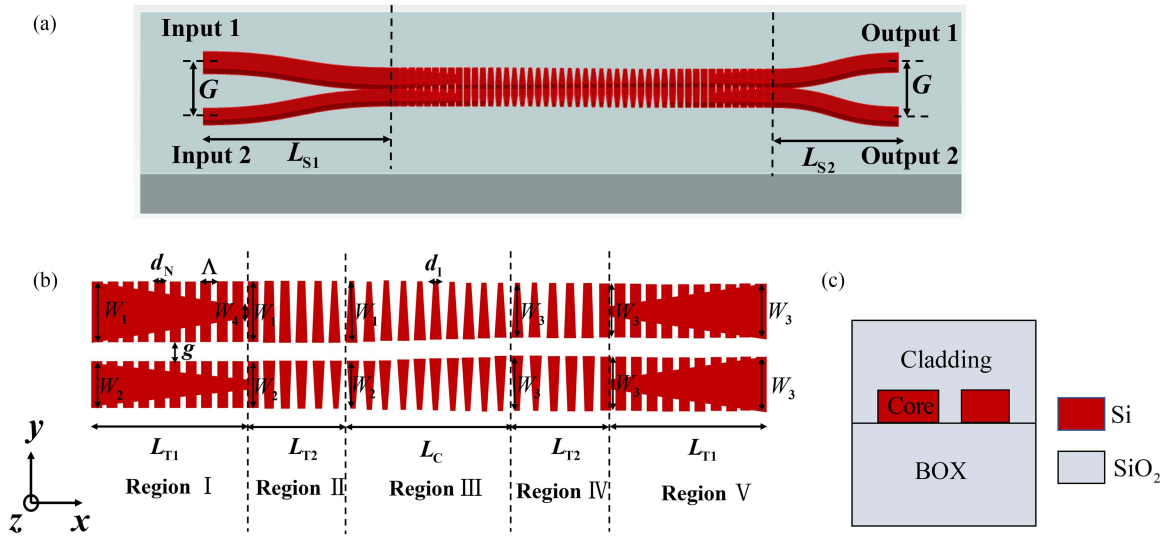

Fig. 1. (a) 3D perspective view (b) top view of the coupling region and (c) cross-sectional view of the 3-dB adiabatic coupler.

domain (FDTD) method, a short coupling length of 24 μm is obtained and the entire length of the device is 47 μm. Moreover, the simulation results show that in the wavelength range of 1450 nm $\sim$ 1650 nm, power splitting ratio (PSR) better than 3$\pm$0.21 dB and insertion loss (IL) less than 0.19 dB can be achieved.

II. Device Structure

The three dimensional schematic of our proposed adiabatic 3-dB optical coupler is shown in Fig. 1(a). Two S-shaped waveguides with length L_{S1} are connected with the left side of coupling region, which can be considered as the input ports of the entire device. Here, $L_{S1} = 15$ μm is chosen to balance the IL and size of the S-shape waveguide. The gap between two S-shape waveguides in the input region is gradually changed from G to g, and the widths of the Input 1 and Input 2 ports are W_1 and W_2, respectively. Also, two S-shaped waveguides with length L_{S2} are connected with the right side of coupling region, which can be considered as the output ports of the entire device, and $L_{S2} = 8$ μm is chosen to minimize the IL and unwanted coupling between two S-shaped waveguides. The gap size between two S-shape waveguides in the output region is gradually changed from g to G, $G = 2$ μm is chosen to avoid coupling between the Output 1 and the Output 2 ports, whose widths are both W_3. For the proposed 3-dB adiabatic coupler, typical silicon waveguide with 220 nm thick top silicon layer, 3 μm thick top and buried SiO_2 layers are used, as shown in Fig. 1(c).

The coupling region consists of five parts, as shown in Fig. 1(b). Region I consists of two waveguide converters, and each of them is made of a stripe waveguide with its width linearly tapered from W_1 (or W_2) to W_4 and a conventional rectangular SWG waveguide with constant width W_1 (or W_2). The length of region I is L_{T1}, the period of the SWG is Λ and the length of the silicon portion in the SWG is d_N. In the region II, gradually varying trapezoidal silicon blocks are adopted to convert two conventional rectangular SWG waveguides to two trapezoidal SWG waveguides. The length of region II is L_{T2}. The width of the trapezoidal SWG waveguides is W_1 (or W_2), the length of the long parallel side of the trapezoidal SWG is d_N while the short one is linearly tapered from d_N to d_l along the propagation direction. The length of region III is L_C, which also consists of two trapezoidal SWGs, whose width is linearly tapered from W_1 (or W_2) to W_3, and the long and short parallel sides of the trapezoidal SWG waveguides are d_N and d_l, respectively. Region IV uses gradually varying trapezoidal SWG waveguides to convert two trapezoidal SWG waveguides to two conventional rectangular SWG waveguides. The length of region IV is L_{T2}. The widths of two trapezoidal waveguides are W_3 and the length of the long parallel side of the trapezoidal SWG waveguides is d_N while the short one is linearly tapered from d_l to d_N. Region V consists of two waveguide converters and each of them consists of a stripe waveguide with its width linearly tapered from W_4 to W_3 and a rectangular SWG waveguide with constant width W_3. The length of region V is L_{T1}, the period of SWG is Λ and the length of silicon portion in the SWG waveguide is d_N. The gap size of the whole coupling region is fixed and denoted as g.

For our 3-dB adiabatic optical coupler, the lowest order even mode will be excited in the coupling region when light is injected into the Input 1 port. The lowest order even mode will be maintained and other modes will not be excited as long as the length of coupling region is sufficiently long. At the end of the coupling region, the optical power will be evenly split between the two output waveguides, which achieves a 3-dB optical power splitting at the output ports. In this situation, the phase difference between the two output ports is zero due to the symmetry of the lowest order even mode. On the other hand, the lowest odd mode will be excited in the coupling region when light is injected into the Input 2 port. Similarly, the lowest order odd mode will be maintained in the coupling region, and the optical power will be evenly split at the end of the coupling region to achieve a 3-dB optical power splitting at the output ports. Under this circumstance, the phase difference between the two output ports is 180° due to the anti-symmetry of the lowest order odd mode.

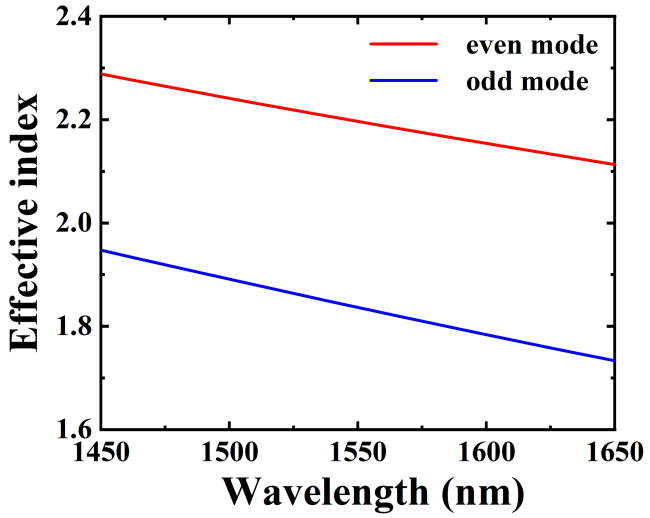

Fig. 2. Simulated effective indices of the lowest order even mode and the lowest order odd mode as a function of wavelength.

III. Simulation Results

In order to avoid unwanted coupling between the Input 1 and Input 2 ports, a sufficiently large waveguide asymmetry is required. Here, $W_1 = 600$ nm and $W_2 = 400$ nm are chosen and the widths of two SWG waveguides in the region V are both set as $W_3 = 500$ nm to achieve 3-dB optical power splitting. For the waveguide converters in region I and region V, the smaller W_4 is, the smaller the loss caused by mode transformation when $W_{\rm i}$ (i = 1-3), Λ and $d_{\rm N}$ are fixed. Here, $W_4 = 100$ nm is chosen so that our design will be compatible with advanced complementary metal-oxide-semiconductor fabrication technologies [30]. For the coupling region, the smaller g is, the shorter coupling region can be, we also set $g = 100$ nm to meet the fabrication technologies. For trapezoidal SWG waveguide, we set $d_{\rm l} = 100$ nm and $d_{\rm N} = 200$ nm respectively to concentrate the light on the lower (upper) side of the upper (lower) waveguide, and Λ is set as 250 nm. We use three-dimensional finite-difference-time-domain (3D FDTD) method to optimize the remaining design parameters and evaluate the performance of our designed 3-dB adiabatic coupler.

It is hereby proved the rationality of Λ. For the grating period Λ, it must be small enough so that the Bragg wavelength is below the minimum operating wavelength to avoid Bragg reflection, which can be ensured by setting $\Lambda < \lambda_{\rm min}/(2\times n_{\rm Bloch})$, where $\lambda_{\rm min}$ is the minimum operating wavelength, and $n_{\rm Bloch}$ is the effective index of the fundamental Floquet-Bloch mode at $\lambda_{\rm min}$. We use 3D FDTD band structure calculations with the Bloch boundary condition to calculate the effective index of Floquet-Bloch mode, and the simulated effective indices of the lowest order even mode and the lowest odd mode as a function of wavelength are shown in Fig. 2. For the lowest order even mode at $\lambda_{\rm min} = 1450$ nm, $n_{\rm Bloch} = 2.29$ is obtained and the maximum value of Λ is given as $\lambda_{\rm min}/(2\times n_{\rm Bloch}) = 1450$ nm/ $(2\times 2.29) = 316.59$ nm, so the choice of $\Lambda = 250$ nm is reasonable.

In order to balance the loss and length of region I and region V, the structure shown in Fig. 3(a) is used to optimize the $L_{\rm T1}$.

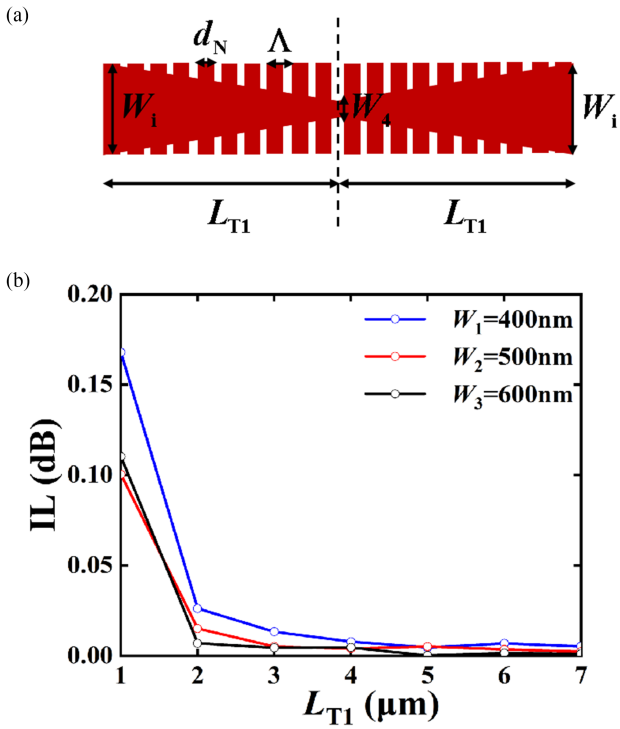

Fig. 3. (a) Structure used to optimize $L_{\rm T1}$ and (b) the ILs as a function of $L_{\rm T1}$ with different $W_{\rm i}$.

The structure consists of two tapered stripe waveguides and two conventional rectangular SWG waveguides. The lengths of two tapered waveguide are $L_{\rm T1}$, the left stripe waveguide with width $W_{\rm i}$ (i = 1-3) is linearly tapered to width W_4 and the right stripe waveguide with width W_4 is linearly tapered to width $W_{\rm i}$. Due to the symmetry of Fig. 3(a), the mode transition loss can be regarded as half of the IL of the structure. The obtained ILs of the structure with different $W_{\rm i}$ as a function of $L_{\rm T1}$ at the wavelength of 1550 nm are shown in Fig. 3(b). As can be seen, the longer that $L_{\rm T1}$ is, the smaller the loss caused by the mode transition between the stripe waveguide and the conventional rectangular SWG waveguide. We set $L_{\rm T1} = 4$ μm to balance the mode transitional loss and length in region I and region V.

Similarly, the structure shown in Fig. 4(a) is used to optimize the $L_{\rm T2}$ of region II and region IV, which consists of two waveguide converters and two gradually varying trapezoidal SWG waveguides. The lengths of two waveguide converters are $L_{\rm T1}$ and each waveguide converter is made of a tapered stripe waveguide and a rectangular SWG waveguide. The left stripe waveguide with width $W_{\rm i}$ (i = 1-3) is linearly tapered to width W_4 and the right stripe waveguide with width W_4 is linearly tapered to width $W_{\rm i}$. The obtained ILs of the structure with different $W_{\rm i}$ as a function of $L_{\rm T2}$ at the wavelength of 1550 nm are shown in Fig. 4(b). As can be seen, the longer $L_{\rm T2}$ is, the smaller the loss caused by the mode transition between the conventional rectangular SWG waveguide and the trapezoidal SWG waveguide. In order to balance the mode conversion loss and length, we set $L_{\rm T2} = 4$ μm to minimize the mode transitional loss in region II and region IV.

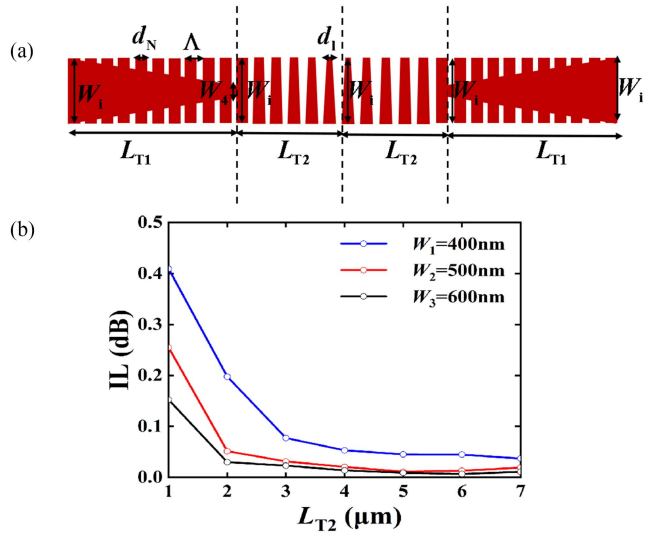

Fig. 4. (a) Structure used to optimize L_{T2} and (b) the ILs as a function of L_{T2} with different W_i.

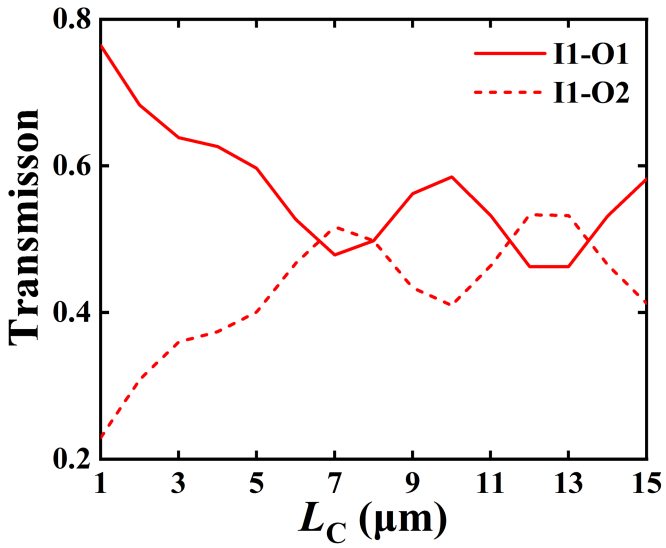

Fig. 5. Transmission at the output ports as a function of L_C.

After L_{T1} and L_{T2} are optimized as 4 μm, then the entire device shown in the Fig. 2(a) is adopted to optimize L_C of region III. When 1550 nm light is injected into the Input 1 port, the simulated transmissions at two output ports as a function of L_C are shown in Fig. 5. Since the device functions as a 3-dB coupler when two curves are intersected, $L_C = 6.5$ μm, 8 μm, 11.5 μm, and 13.5 μm can be selected. In order to shrink the device size, $L_C = 6.5$ μm should be chosen. However, we set $L_C = 8$ μm to achieve evenly power splitting in a broad working bandwidth.

Table I summarizes all the optimized parameters of our 3-dB adiabatic coupler based on trapezoidal SWG.

When 1550 nm light is injected into the Input 1 and Input 2 ports, the simulated electric field distributions are shown in the upper and lower parts of Fig. 6, respectively. As can be seen, when light is injected into the Input 1 port, the lowest order even mode is excited in the coupling region, and the optical power

TABLE I
LIST OF OPTIMIZED PARAMETERS FOR THE 3-DB ADIABATIC COUPLER BASED ON TRAPEZOIDAL SWG

W_1	W_2	W_3	W_4	d_1	d_N	Λ
600nm	400nm	500nm	100nm	100nm	200nm	250nm
g	G	L_{S1}	L_{S2}	L_{T1}	L_{T2}	L_C
100nm	2μm	15μm	8μm	4μm	4μm	8μm

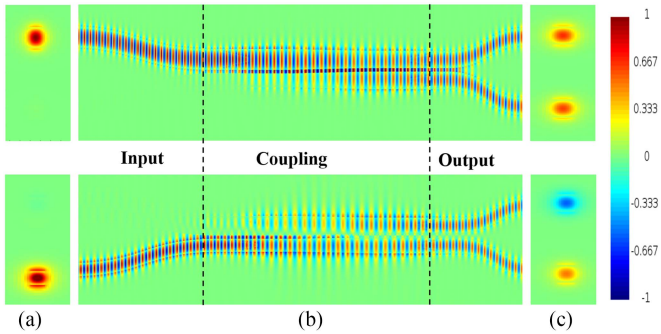

Fig. 6. (a) Input view; (b) top view; (c) output view of the simulated electric field distribution at 1550 nm wavelength.

is split into two output ports evenly with zero phase difference. On the other hand, when light is injected into the Input 2 port, the lowest order odd mode in the coupling region is excited and the optical power is split into two output ports evenly with 180° phase difference.

Finally, the simulated PSR and IL as a function of wavelength are shown in Fig. 7(a) and (b), respectively. The PSR and IL are defined as:

$$\mathrm{PSR} = 10\lg\frac{P_i}{\sum P_i}(dB) \tag{1}$$

$$\mathrm{IL} = -10\lg\sum P_i(dB),\ i = 1, 2 \tag{2}$$

where P_1 and P_2 are the output power of the Output 1 and Output 2 ports, respectively. In the wavelength range of 1450 nm $\sim$ 1650 nm, the obtained PSR is better than 3$\pm$0.21 dB and the IL is less than 0.03 dB when light is injected into the Input 1 port. And PSR is better than 3$\pm$0.21 dB and the IL is less than 0.19 dB when light is injected into the Input 2 port. When light is injected into the Input 1 port, the electric field distribution in simulation area does not change much at different wavelengths, so the loss shows small fluctuations over wavelength. However, when light is injected into the Input 2 port, the scattering in the simulation area increases significantly with wavelength, so the loss is also much increased. The simulation results indicate that our device achieves an almost adiabatic mode evolution.

The fabrication tolerance is also explored by simulating the coupler with some fabrication variations (Δh, ΔW, and Δd_N), where Δh is the waveguide thickness variation, ΔW is the waveguide width variation and the Δd_N is the length variation of the long parallel side of the trapezoidal SWG. Here the coupling region g and the period of the SWG Λ are kept constant. When light is injected into the Input 1 Port, the simulated PSRs as a function of wavelength are shown in the Fig. 8(a)–(c), the

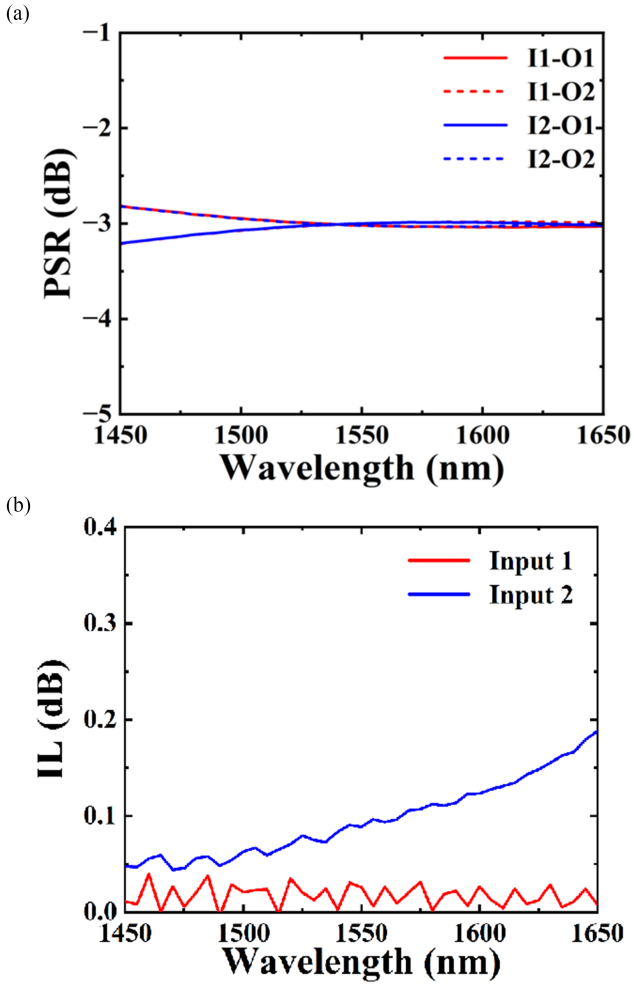

Fig. 7. Simulated (a) PSR and (b) IL for the 3-dB adiabatic coupler in the wavelength range of 1450 nm ∼ 1650 nm.

obtained PSRs are better than −3±0.44 dB when there is a fabrication variation of $\Delta h = \pm 10$ nm, $\Delta W = \pm 10$ nm or $\Delta d_{\mathrm{N}} = \pm 10$ nm. The ILs are also calculated, which are also less than 0.05 dB. Therefore, our design has good tolerance to possible fabrication variations in the wavelength range of 1450 nm to 1650 nm.

Due to fabrication errors and other factors, experimental results are usually worse than simulated results, but simulation is still an important method to design device with high performance. We also conduct a performance comparison based on the reported simulation results. Table II summarizes the simulated performance of our device and approximate simulated results of several reported 3-dB adiabatic couplers. It shows that the proposed 3-dB adiabatic coupler based on the trapezoidal SWG has shorter length than adiabatic couplers based on the conventional rectangular SWG [21], [22], [23]. Also, it is shorter than most adiabatic couplers based on conventional stripe/ridge waveguide [10], [11], [16], [17], [18] and almost same as Ref. [12]. However, our device can achieve even power splitting in a broader working bandwidth than Ref. [12].

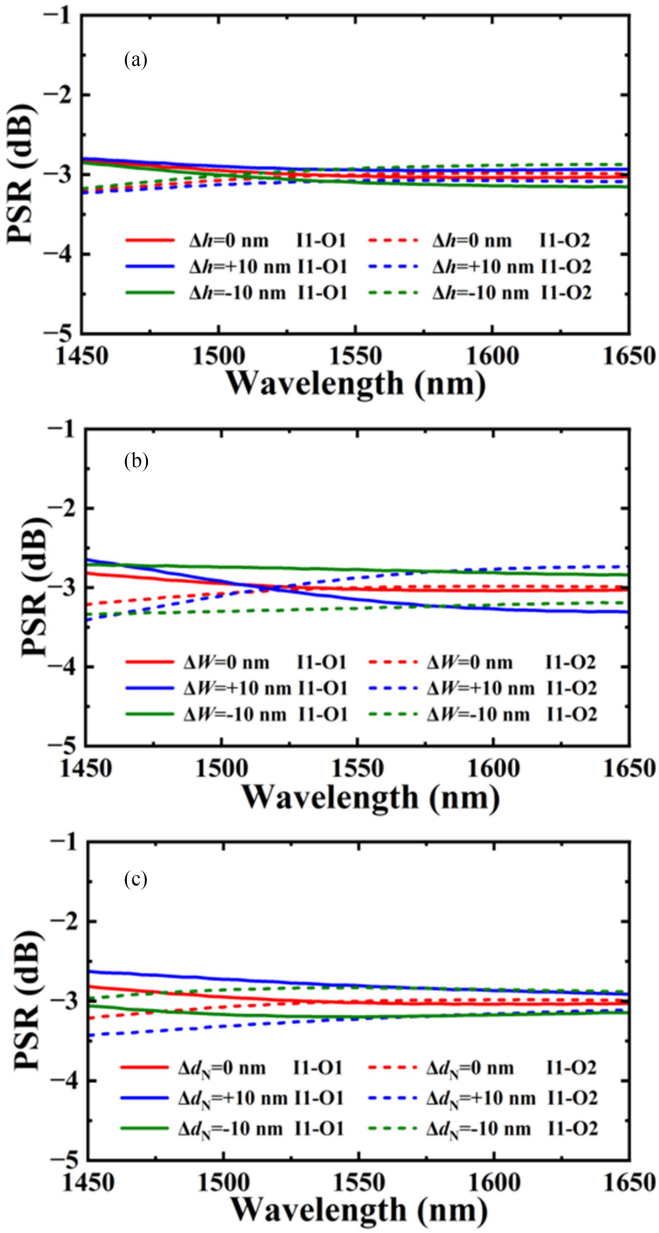

Fig. 8. Simulated PSRs for the 3-dB adiabatic coupler with some fabrication variations. (a) $\Delta h = \pm 10$ nm; (b) $\Delta W = \pm 10$ nm; and (c) $\Delta d_{\mathrm{N}} = \pm 10$ nm.

TABLE II
COMPARISON OF OUR DEVICE WITH REPORTED 3-DB ADIABATIC COUPLERS

Reference	Coupling Length (μm)	Total Length (μm)	PSR(dB)	Bandwidth (nm)	IL (dB)
[10]	300	/	3±0.15	200	/
[11]	90	/	3±0.5	200	/
[12]	23.2	46.7	3±0.18	135	<0.1
[16]	60	~70	3±0.15	165	<0.14
[17]	26.3	68.3	3±0.5	100	/
[18]	45	105	3±0.24	100	~0
[21]	50	80	/	180	/
[22]	35	/	3±0.75	500	<0.012
[23]	25	65	3±0.33	100	<0.08
This	24	47	3±0.21	200	<0.19

IV. Conclusion

In summary, we have proposed a compact, broadband 2×2 3-dB adiabatic coupler based on trapezoidal SWG on SOI platform. It is shorter than adiabatic couplers based on conventional rectangular SWG and most adiabatic couplers based on conventional stripe/ridge waveguide. Moreover, it can achieve even power splitting in a broad working bandwidth. The coupling length and total length of our device are only 24 μm and 47 μm, respectively. The simulated results show that PSR better than 3±0.21 dB and IL less than 0.19 dB in the wavelength range of 1450 nm $\sim$ 1650 nm can be achieved, which is very promising for broadband applications.

References

[1] M. R. Watts et al., "Adiabatic thermo-optic Mach-Zehnder switch," *Opt. Lett.*, vol. 38, no. 5, pp. 733–735, 2013, doi: 10.1364/OL.38.000733.

[2] B. Lin et al., "Dual-mode 2 × 2 thermo-optic switch based on polymer waveguide Mach-Zehnder interferometer," *IEEE Photon. Technol. Lett.*, vol. 34, no. 24, pp. 1317–1320, Dec. 2022, doi: 10.1109/LPT.2022.3214579.

[3] F. Horst et al., "Cascaded Mach-Zehnder wavelength filters in silicon photonics for low loss and flat pass-band WDM (de-)multiplexing," *Opt. Exp.*, vol. 21, no. 10, pp. 11652–11658, 2013, doi: 10.1364/OE.21.011652.

[4] C. Sun, Y. Yu, M. Ye, G. Chen, and X. Zhang, "An ultra-low crosstalk and broadband two-mode (de)multiplexer based on adiabatic couplers," *Sci. Rep.*, vol. 6, no. 1, Dec. 2016, Art. no. 38494, doi: 10.1038/srep38494.

[5] L. Zhang, S. Jie, and J. Xiao, "Broadband and scalable silicon-based mode multiplexer using subwavelength-grating-based adiabatic coupler," *J. Nanophotonics*, vol. 15, no. 4, Oct. 2021, Art. no. 046010, doi: 10.1117/1.JNP.15.046010.

[6] Z. Lu et al., "Broadband silicon photonic directional coupler using asymmetric-waveguide based phase control," *Opt. Exp.*, vol. 23, no. 3, pp. 3795–3808, 2015, doi: 10.1364/OE.23.003795.

[7] R. K. Gupta, S. Chandran, and B. K. Das, "Wavelength-independent directional couplers for integrated silicon photonics," *J. Lightw. Technol.*, vol. 35, no. 22, pp. 4916–4923, Nov. 2017, doi: 10.1109/JLT.2017.2759162.

[8] K. Solehmainen, M. Kapulainen, M. Harjanne, and T. Aalto, "Adiabatic and multimode interference couplers on silicon-on-insulator," *IEEE Photon. Technol. Lett.*, vol. 18, no. 21, pp. 2287–2289, Nov. 2006, doi: 10.1109/LPT.2006.885305.

[9] K. A. Latunde-Dada and F. P. Payne, "Theory and design of adiabatically tapered multimode interference couplers," *J. Lightw. Technol.*, vol. 25, no. 3, pp. 834–839, Nov. 2007, doi: 10.1109/JLT.2006.889678.

[10] J. Xing et al., "Silicon-on-insulator-based adiabatic splitter with simultaneous tapering of velocity and coupling," *Opt. Lett.*, vol. 38, no. 13, pp. 2221–2223, 2013, doi: 10.1364/OL.38.002221.

[11] I. K. Kim, V. Nguyen, and T. J. Seok, "2x2 silicon photonic 3-dB adiabatic coupler with optimized taper curvature," in *Proc. Int. Conf. Opt. MEMS Nanophotonics* , 2019, pp. 218–219.

[12] I. K. Kim, D. U. Kim, V. H. Nguyen, S. Han, and T. J. Seok, "High-performance and compact silicon photonic 3-dB adiabatic coupler based on shortest mode transformer method," *IEEE Photon. J.*, vol. 13, no. 4, Aug. 2021, Art. no. 6601106, doi: 10.1109/JPHOT.2021.3107852.

[13] D. Mao et al., "Adiabatic coupler with nonlinearly tapered mode-evolution region," *IEEE Photon. Technol. Lett.*, vol. 33, no. 16, pp. 840–843, Aug. 2021, doi: 10.1109/LPT.2021.3072787.

[14] H. Chung, C. Chen, Y. Hung, and S. Tseng, "Compact polarization-independent quasi-adiabatic 2×2 3 dB coupler on silicon," *Opt. Exp.*, vol. 30, no. 2, pp. 995–1002, 2022, doi: 10.1364/OE.446492.

[15] X. Liu et al., "Compact, ultrabroadband and temperature-insensitive arbitrary ratio power splitter based on adiabatic rib waveguides," *Appl. Opt.*, vol. 62, no. 5, pp. 1279–1284, 2023, doi: 10.1364/AO.479304.

[16] D. Guo and T. Chu, "Compact broadband silicon 3 dB coupler based on shortcuts to adiabaticity," *Opt. Lett.*, vol. 43, no. 19, pp. 4795–4798, 2018, doi: 10.1364/OL.43.004795.

[17] Y. J. Hung et al., "Mode-evolution-based silicon-on-insulator 3 dB coupler using fast quasiadiabatic dynamics," *Opt. Lett.*, vol. 44, no. 4, pp. 815–818, 2019, doi: 10.1364/OL.44.000815.

[18] L. Xu et al., "Broadband 2×2 adiabatic 3-dB coupler with inversely-tapered mode-evolution region for the silicon-on-insulator platform," in *Proc. IEEE Photon. Conf.*, 2020, pp. 1–2.

[19] Y. Wang et al., "Compact broadband directional couplers using subwavelength gratings," *IEEE Photon. J.*, vol. 8, no. 3, Jun. 2016, Art. no. 7101408, doi: 10.1109/JPHOT.2016.2574335.

[20] A. Ortega-Moñux et al., "An ultra-compact multimode interference coupler with a subwavelength grating slot," *Laser Photon. Rev.*, vol. 7, no. 2, pp. L12–L15, 2013, doi: 10.1002/lpor.201200106.

[21] H. Yun et al., "Broadband 2 × 2 adiabatic 3 dB coupler using silicon-on-insulator sub-wavelength grating waveguides," *Opt. Lett.*, vol. 41, no. 13, pp. 3041–3044, 2016, doi: 10.1364/OL.41.003041.

[22] H. Yun, L. Chrostowski, and N. Jaeger, "Ultra-broadband 2 × 2 adiabatic 3 dB coupler using subwavelength-grating-assisted silicon-on-insulator strip waveguides," *Opt. Lett.*, vol. 43, no. 8, pp. 1935–1938, 2018, doi: 10.1364/OL.43.001935.

[23] L. H. Xu et al., "Compact high-performance adiabatic 3-dB coupler enabled by subwavelength grating slot in the silicon-on-insulator platform," *Opt. Exp.*, vol. 26, no. 23, pp. 29873–29885, 2018, doi: 10.1364/OE.26.029873.

[24] Y. Xu and J. Xiao, "Compact and high extinction ratio polarization beam splitter using subwavelength grating couplers," *Opt. Lett.*, vol. 41, no. 4, pp. 773–776, 2016, doi: 10.1364/OL.41.000773.

[25] M. B. Mia, S. Z. Ahmed, I. Ahmed, N. Jaidye, and S. Kim, "Ultra-broadband silicon photonic polarization beam splitter with anisotropic subwavelength grating metamaterials," in *Proc. IEEE Photon. Conf.*, 2021, pp. 1–2.

[26] H. Xu and Y. Shi, "Ultra-sharp multi-mode waveguide bending assisted with metamaterial-based mode converters," *Laser Photon. Rev.*, vol. 12, no. 3, Mar. 2018, Art. no. 1700240, doi: 10.1002/lpor.201700240.

[27] H. Wu et al., "Ultra-sharp multimode waveguide bends with subwavelength gratings," *Laser Photon. Rev.*, vol. 13, no. 2, Feb. 2019, Art. no. 1800119, doi: 10.1002/lpor.201800119.

[28] J. M. Luque González et al., "An ultracompact grin-lens-based spot size converter using subwavelength grating metamaterials," *Laser Photon. Rev.*, vol. 13, no. 11, Nov. 2019, Art. no. 1900172, doi: 10.1002/lpor.201900172.

[29] L. Sun, R. Hu, Z. Zhang, Y. He, and Y. Su, "Ultrabroadband power coupling and mode-order conversion based on trapezoidal subwavelength gratings," *IEEE J. Sel. Top. Quantum Electron.*, vol. 27, no. 6, Nov./Dec. 2021, Art. no. 8100308, doi: 10.1109/JSTQE.2021.3092383.

[30] S. K. Selvaraja et al., "193nm immersion lithography for high-performance silicon photonic circuits," *Proc. SPIE*, vol. 9052, 2014, Art. no. 90520F.